SAND2019-14576C

Extending the Frequency Limits of "Postage-Stamp PIV" to MHz Rates

Steven J. Beresh,[1] Russell W. Spillers,[2] Melissa M. Soehnel,[3] and Seth M. Spitzer[4]
Sandia National Laboratories, Albuquerque, NM, 87185

Two techniques have extended the effective frequency limits of postage-stamp PIV, in which a pulse-burst laser and very small fields of view combine to achieve high repetition rates. An interpolation scheme reduced measurement noise, raising the effective frequency response of previous 400-kHz measurements from about 120 kHz to 200 kHz. The other technique increased the PIV acquisition rate to very nearly MHz rates (990 kHz) by using a faster camera. Charge leaked through the camera shift register at these framing rates but this was shown not to bias the measurements. The increased framing rate provided oversampled data and enabled use of multi-frame correlation algorithms for a lower noise floor, increasing the effective frequency response to 240 kHz where the interrogation window size begins to spatially filter the data. Good agreement between the interpolation technique and the MHz-rate PIV measurements was established. The velocity spectra suggest turbulence power-law scaling in the inertial subrange steeper than the theoretical -5/3 scaling, attributed to an absence of isotropy.

Introduction

The measurement of turbulent velocity spectra in high-speed flows requires that very high frequencies must be reached at small spatial scales. The most common means of measuring velocity spectra such as hot-wire anemometry [1, 2] and laser Doppler velocimetry [3, 4] generally fail to achieve the necessary frequency response, which can require 100 kHz or more. In contrast, time-resolved particle image velocimetry (TR-PIV) using a pulse-burst laser recently has demonstrated an ability to directly measure spectral content at very high frequencies without need for any frozen turbulence assumptions [5, 6]. The laser energy available at high frequencies is considerably reduced and must be confined to a small field of view if sufficient scattered energy is to be collected. Current high-speed camera technology allows very fast image acquisition for long time sequences if the field of view is windowed down to a small array. Combining these approaches, pulse-burst PIV was acquired by Beresh et al [6] at 400 kHz for image sequences exceeding 4,000 frames, but by necessity for a small array of only 128 × 120 pixels, giving rise to the moniker of "postage-stamp PIV."

Still, the postage-stamp PIV data reached frequency limitations of approximately 120-130 kHz due to interference from the noise floor of the measurement. To accurately measure the highest frequencies that can be delivered by postage-stamp PIV and detect the turbulent phenomena that motivate the technique, a noise reduction scheme was explored [7]. The need for such denoising algorithms has been evident in low-speed applications of TR-PIV, but the approaches that have been developed [8-10] were found unsuitable to the present case. Either an assumed spectral form is required [9] or an accurate estimate of the noise floor must be produced from oversampled data [10], neither of which is suitable to the high-speed flows for which postage-stamp PIV is intended. Moreover, the

---

[1] Distinguished Member of the Technical Staff, Engineering Sciences Center, AIAA Associate Fellow, correspondence to: P.O. Box 5800, Mailstop 0825, (505) 844-4618, email: sjberes@sandia.gov

[2] Principal Technologist, Engineering Sciences Center

[3] Test Operations Engineer, Engineering Sciences Center

[4] Technologist, Engineering Sciences Center

Sandia National Laboratories is a multi-mission laboratory managed and operated by National Technology and Engineering Solutions of Sandia, LLC., a wholly owned subsidiary of Honeywell International, Inc., for the U.S. Department of Energy's National Nuclear Security Administration under contract DE-NA0003525.

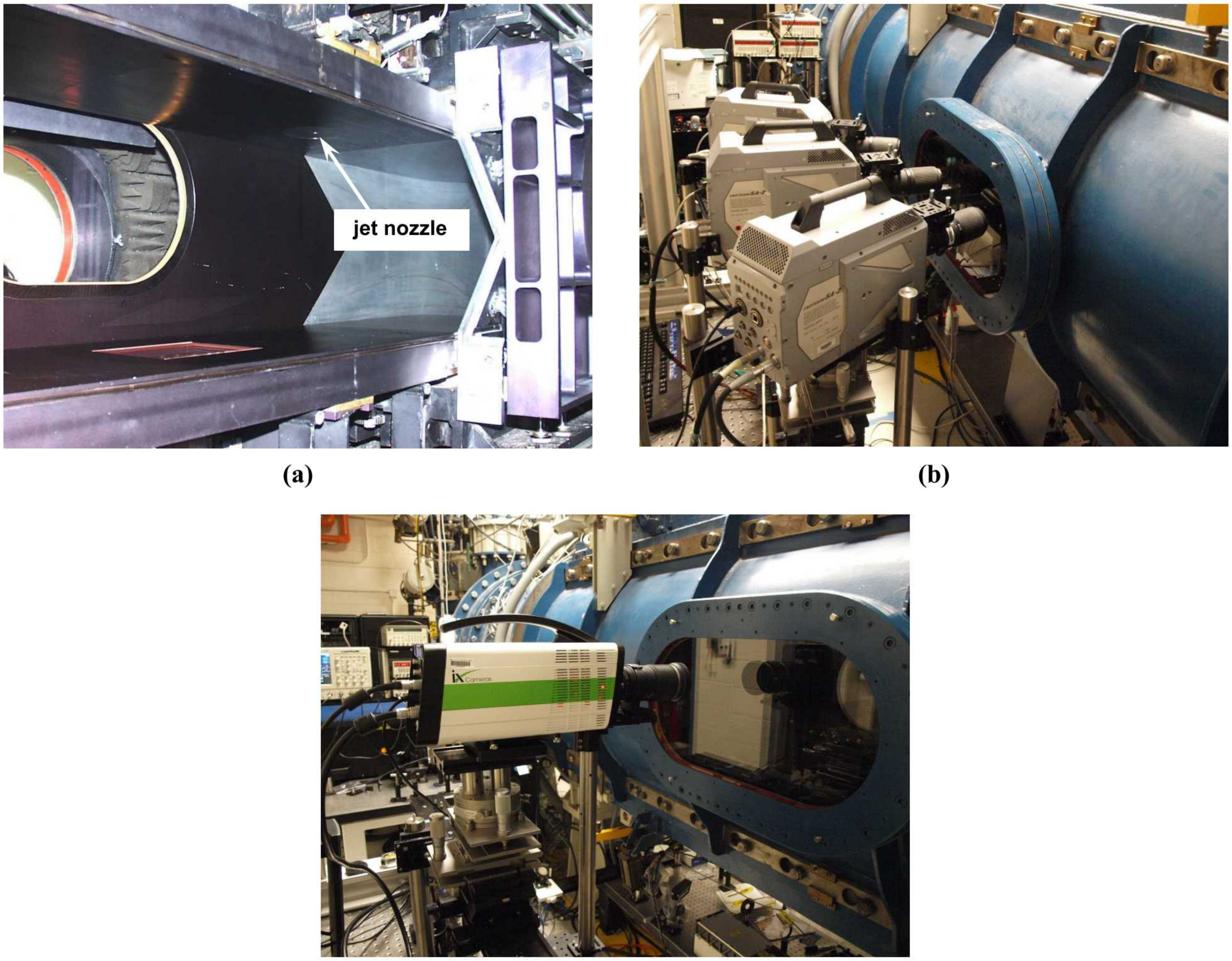

(a) (b)

(c)

Fig. 1: Photo of the experimental configurations. (a) The jet-in-crossflow experiment. (b) The SA-Z camera setup for the previous postage-stamp PIV measurements. (c) The IX 726 camera setup for MHz-rate postage-stamp PIV measurements.

algorithms are predicated on an assumption that PIV noise is white noise [8, 10], which was shown to be inaccurate [7]. Denoising via uncertainty [11] also was unsuccessful, likely because uncertainty is only a bound on the possible error, not the actual error of the measurement.

Therefore, postage-stamp PIV remains in need of a means of increasing its effective frequency limitation due to the noise floor. The present paper develops two means of accomplishing this. The first of these employs an interpolation scheme based upon the temporal super-sampling of Scarano and Moore [12]. By drawing measurements from multiple spatial and temporal locations, errors that are not spatially correlated will average out and the noise floor is decreased. The second approach is simply to use the increased speeds of the most recently available cameras to obtain data at a sampling rate of 990 kHz. Previous MHz-rate pulse-burst PIV systems have been developed by Wernet and Opalski [13] and by Brock et al [14], but these could only acquire 8 and 14 images, respectively, and therefore were unsuited to obtaining spectral content. But to achieve such high imaging rates for long sequences, the cameras possess drawbacks that can have unfortunate properties for accurate PIV measurements. Nevertheless, both methods show an ability to raise the effective frequency response of postage-stamp PIV and are detailed herein.

Experimental Configuration

Previous 400-kHz Postage-Stamp PIV Measurements

A brief description of postage-stamp PIV is provided here, with the full details to be found in Beresh et al [6].

The development of postage-stamp PIV has been performed using a supersonic jet exhausting into a transonic crossflow, identically to previous efforts [5, 6]. This work was conducted in Sandia's Trisonic Wind Tunnel (TWT), which is a blowdown-to-atmosphere facility using air as the test gas through a test section of dimensions 305 × 305 mm^2 (12 × 12 inch^2). Mach 0.8 was tested exclusively for the data used herein at a fixed stagnation pressure of 154 kPa and stagnation temperature of 321K ± 2K. A supersonic jet was installed on the top wall of the test section upstream of the windows, as seen in Fig. 1a, for measurement of the far-field of the jet interaction. The laser sheet was introduced through a window in the floor of the test section and was oriented in the streamwise plane and aligned to the center plane of the test section, which coincides with the center of the jet nozzle exit. A nitrogen jet exhausted from a conical nozzle with a design Mach number of 3.73, an expansion half-angle of 15 deg, and an exit diameter of 9.53 mm. In the present case, the jet was operated at a pressure of 3.9 MPa to produce a jet-to-freestream dynamic pressure ratio of J=8.1. The coordinate axes originate at the centerpoint of the nozzle exit plane; the u component is in the streamwise direction and v component is positive away from the top wall of the tunnel.

The TWT is seeded by a thermal smoke generator (Corona Vi-Count 5000) whose output is delivered to the TWT's stagnation chamber upstream of the flow conditioning section through a series of pipes and tubes, in which agglomeration of the particles occurs. Previous measurement of the *in-situ* particle response across a shock wave generated by a wedge showed the particle size to be 0.7 - 0.8 μm. Stokes numbers have been estimated as at most 0.05 based on *a posteriori* analysis of PIV measurements, which is sufficiently small to render particle lag errors negligible.

A burst-mode laser (QuasiModo-1000, Spectral Energies, LLC) with both diode- and flashlamp-pumped Nd:YAG amplifiers was used to produce a high-energy pulse train at 532 nm. The pulse-burst laser generates a burst of maximum duration 10.2 ms once every 8 seconds with a maximum repetition rate of 500 kHz. For postage-stamp PIV, it was operated to deliver single pulses at 400 kHz with an energy of about 8 mJ per pulse at 532 nm, creating a time between successive pulses of 2.5 μs. The laser sheet was narrowed to a slender width to concentrate the available energy in the small field of view and had a sheet thickness of 1 mm. A total of about 150 bursts of data were acquired.

Images were acquired using high-speed CMOS cameras (Photron SA-Z) which have an array of 1024 × 1024 pixels at a full framing rate of 20 kHz. Their windowing function allows the framing rate to be increased by sampling a semi-arbitrary portion of the imaging array. The SA-Z cameras were operated at 400 kHz, which necessitates that they are windowed down to a small array of only 128 × 120 pixels; hence the use of the term "postage-stamp PIV."

Three SA-Z cameras were used to acquire two independent measurements, as seen in Fig. 1b. One camera was aligned for a conventional two-component measurement whereas the other two cameras combined for a stereoscopic measurement. The cameras each were equipped with 200-mm focal length lenses and anti-peak-locking diffuser plates [15]. The present work considers only the two-component measurements.

Data were processed using LaVision's DaVis v8.3.1 or v8.4.0. In each case, image pairs were background corrected, intensity normalized, and then interrogated with an initial pass using 64 × 64 pixel interrogation windows, followed by two iterations of Gaussian-weighted 24 × 24 pixel interrogation windows. A 50% overlap in the interrogation windows was used as well. The resulting vector fields were validated based upon signal-to-noise ratio, nearest-neighbor comparisons, allowable velocity range, and a median filter in both space and time.

MHz-Rate Postage-Stamp PIV Measurements

Since the original postage-stamp PIV measurements were published, IX Cameras released the model IX 726, which is capable of reaching a framing rate of 1 MHz with windowed arrays similarly to the Photron SA-Z that was used previously. The IX 726 also is a CMOS camera, in this case with a native resolution of 2048 × 1536 digitized at 12 bits. A single IX 726 for two-component PIV measurements is shown aligned to the TWT in Fig. 1c.

Unfortunately, the IX 726 cannot be windowed effectively in an approximately square aspect ratio as can the SA-Z. To achieve its high framing rate, the design of the horizontal shift register leaks charge between rows when the horizontal resolution is decreased to small values. Although the IX 726 can operate in a nearly square aspect ratio of 112 × 108 pixels at 1 MHz, it creates serious ghosting problems in the image. These artifacts can have damaging consequences to PIV accuracy when cross-correlations are computed between frames to determine velocity vectors. As the horizontal dimension is increased, the charge leakage and ghosting problems diminish. For the present experiments, the camera was operated in one of two modes, either 336 × 42 pixels or 504 × 30 pixels. The consequences of both the long aspect ratio of the images and the residual charge leakage both are examined as part of the present study.

In addition, the IX 726 has a rigid limit of 1 MHz framing rate in its trigger pulse counter. Due to small discrepancies and phase differences between clocks when operating at 1 MHz, it tends to drop frames occasionally and therefore contaminate the image sequences. For this reason, it must be operated at slightly less than 1 MHz. Resolution limitations on the timing pulse generator used for the pulse-burst laser made 990 kHz a sensible choice for

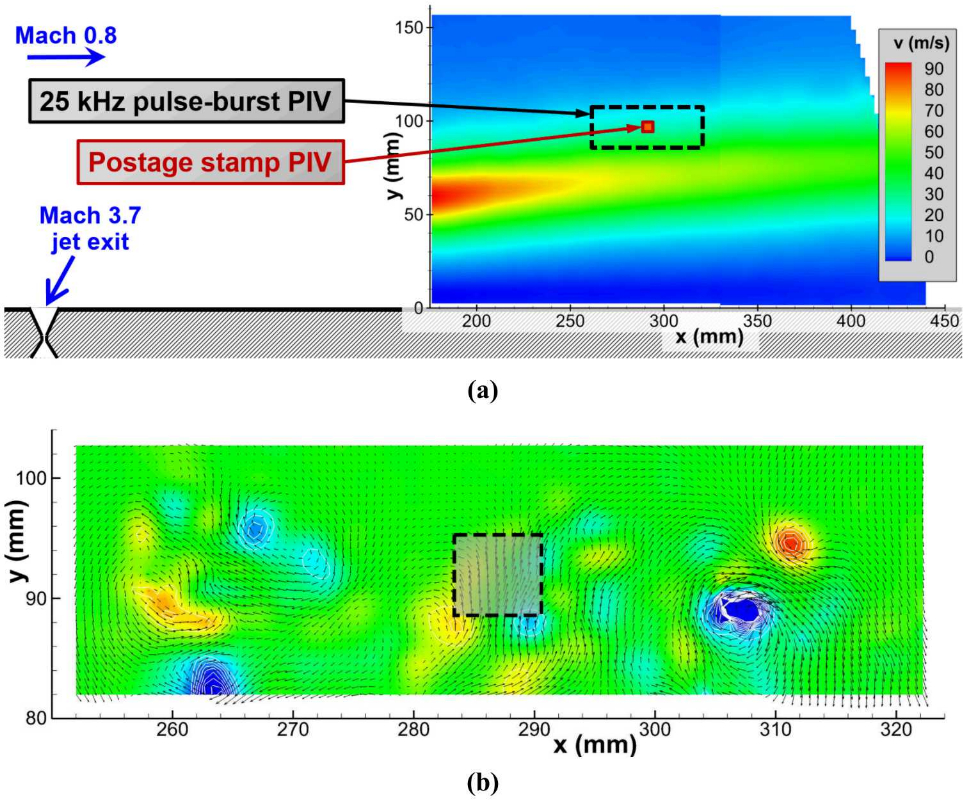

Fig. 2: Field of view of the postage-stamp PIV measurement within the larger jet-in-crossflow experiment superposed on: (a) a conventional PIV mean vector field of the far-field [16], and (b) a snapshot from the earlier 25-kHz pulse-burst PIV data [5].

a pulse rate compatible with both the camera and the laser. These measurements are still termed "MHz-rate" as they are within a small rounding error of 1 MHz.

The pulse-burst laser was modified slightly to produce pulse frequencies of 990 kHz and still achieve adequate laser pulse energy. This was accomplished by shortening the seed pulse duration from 10 ns to 4 ns and by using a tighter telescope to focus the beam on the second-harmonic generator. Both of these modifications improved the conversation efficiency of the doubling process and achieved 5.5 mJ per pulse at 532 nm. The laser was operated for 10.2 ms duration bursts, with 12 seconds required between bursts to dissipate heat sufficiently to maintain reasonable beam quality burst-to-burst.

It should be noted that other very-high-speed cameras exist, such as the Shimadzu HPV-X2, which can reach framing rates of 10 MHz, and the Kirana from Specialized Imaging, which can reach 5 MHz. However, these cameras can only acquire sequences of 256 and 180 images, respectively. Such short record lengths are not suitable for obtaining frequency spectra with a broad range of scales. Although they potentially could be used to measure just the high-frequency spectral regime as a supplement to previous postage-stamp PIV measurements, a very large quantity of image sequences would be required to achieve reasonable convergence of the high-frequency spectra. In combination with the low duty cycle of the pulse-burst laser and the low duty cycle of the blowdown wind tunnel, acquisition of sufficient image sequences is impractical. For this reason, such cameras were deemed inappropriate to the spectral goals of the postage-stamp PIV measurements.

Experimental Results

Previous 400-kHz Postage-Stamp PIV Measurements

The field of view for the postage-stamp PIV is shown in Fig. 2. The full extent of the jet-in-crossflow experiment is given in Fig. 2a using conventional 10-Hz PIV [16], with the vertical component of the mean velocity field shown positioned in its far-field location. Superposed are the fields of view for both the 25-kHz pulse-burst PIV described in [5] and the postage-stamp PIV [6]. Figure 2b reproduces a previous pulse-burst PIV vector field from [5] as well

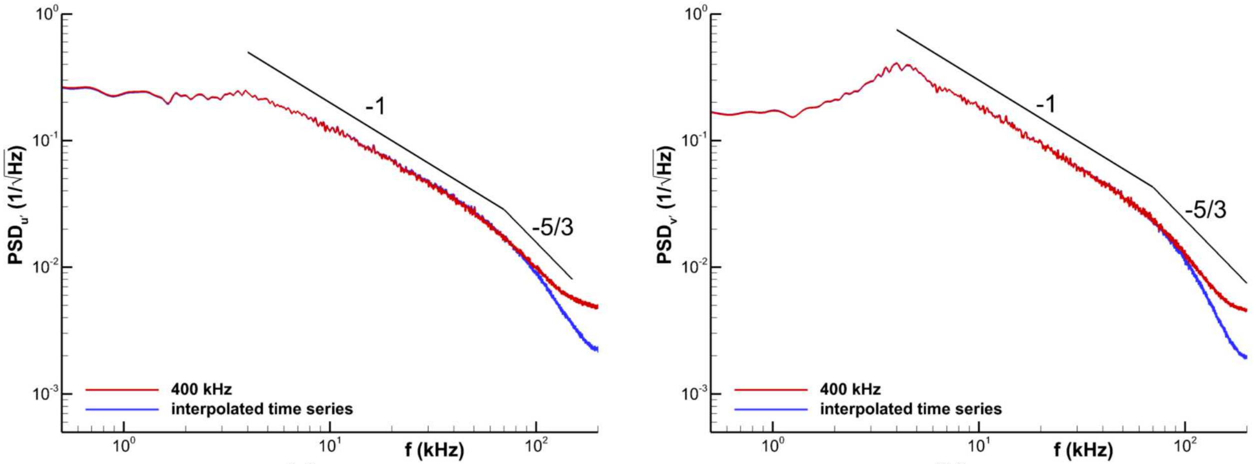

(a) **(b)**

Fig. 3: 400-kHz postage-stamp PIV power spectra of velocity fluctuations for the jet in crossflow [6]. Spectra from the interpolated time series technique also are shown. (a) streamwise component; (b) vertical component.

as the postage-stamp PIV field of view. The small size of the postage-stamp PIV window is evident, little more than a point measurement. This measurement will reveal little about the structure of the flow given its minimal extent, but this is a necessary sacrifice to achieve the very high framing rate that can yield high-frequency spectral content.

The power spectra of the velocity fluctuations that are measured by the two-component postage-stamp PIV are shown in Fig. 3. Two PSD plots are shown, one for the streamwise component of velocity fluctuations and the other for the vertical component. In the present case, the properties of the jet interaction change very little within the far-downstream field of view and it suffices to examine the spectra at a single point near the center of the field of view where no edge effects interfere with computing correlations as particles may exit the field of view. Slopes for -1 and -5/3 power law dependencies are provided as well. Also shown are spectra for the interpolated time series, which will be described subsequently.

For both velocity components in Fig. 3, the spectral content of the flow is visible to high frequencies until the noise floor intrudes at about 120 kHz. The most consequential of the spectra is the vertical component in Fig. 3b. The spectra peak at 4 kHz, which corresponds to one full period between pairs of turbulent eddies convecting through the flow [17]. Following the peak, the spectra then exhibit a -1 slope dependence to about 60-70 kHz before gradually transitioning to an apparent -5/3 slope dependence. The presence of the -5/3 region is well-known and expected as a consequence of the inertial subrange of turbulence decay (e.g., Pope [18]). The -1 dependence, on the other hand, is an unanticipated discovery and lasts for at least one full decade, from approximately 4 – 60 kHz. It is discussed in more detail in [6].

The streamwise component in Fig. 3a also appears to be supportive of a -1 slope dependence but its lack of a peak means this region does not initiate until about 8 kHz. The -5/3 slope dependence at high frequencies is somewhat less convincing for the streamwise component than for the vertical component. This is because the overall intensity of the streamwise velocity fluctuations is reduced compared to the vertical velocity fluctuations, and therefore the impact of the noise floor is felt sooner.

The stereoscopic postage-stamp PIV measurements are not yet used within the context of the present techniques to increase the frequency limits, and hence they are omitted from this paper.

Interpolated Time Series

The 400-kHz velocity spectra shown in Fig. 3 are based upon a single point in the flow. Notwithstanding the small size of the postage-stamp PIV field of view, an 11 × 11 vector field is produced. The additional spatial information provided by the surrounding vectors may offer an opportunity to reduce the noise floor of the measurement. If the high-frequency content of the time-series information is dominated by errors uncorrelated in space, use of multiple vectors may result in a lower noise floor by the power of averaging and therefore yield a higher effective frequency limit. Still, a simple average will not suffice, as this will increase the spatial extent of the measurement and therefore reduce the frequency response. This occurs because the frequency response is coupled to the spatial resolution of the measurement through the local convection velocity.

The time super-sampling technique of Scarano and Moore [12] may offer a plausible means of accomplishing this. They demonstrated a means of extracting considerably higher frequencies of information from TR-PIV than would be indicated by the framing rate of vector fields. In the time between successive velocity fields in a typical TR-PIV system, the flow convects by multiple vector spacings. The intervening vectors contain valid information that may be introduced to the temporal signals. For flows dominated by convection, Taylor's Hypothesis of frozen turbulence may be assumed locally valid over this short distance and time and the local instantaneous convection velocity is used to convert these additional vectors to smaller time steps to fill the temporal gaps between actual data acquisition intervals. Scarano and Moore [12] portray such a super-sampling algorithm as "pouring space into time."

In the present case, the very high framing rate of postage-stamp PIV does not leave additional frequency content in space that can be poured into time to boost the effective frequency response – the flow convects by only a single vector spacing between frames. But nonetheless, Scarano and Moore's time super-sampling technique is applicable. It offers a means of obtaining a single velocity vector from multiple vectors in space and time without averaging them, but the use of multiple points reduces the impact of the noise by the classic $\sqrt{N}$ ratio. By interpolating instead of averaging, it retains the narrow space and time resolution required to achieve a high-frequency measurement. Using a super-sampling factor of 2, which interpolates a single point between measured vector fields, a new spectrum is computed using only the interpolated points and not the native data points. This allows analysis of a functionally equivalent spectrum except it is interpolated from multiple points and thereby reduces the noise floor. These are included in Fig. 3 to be compared to the original spectra.

For both velocity components, the noise floor appears to have been reduced from 0.005 to 0.002, a factor of 2.5 improvement. The interpolation scheme uses four points at each of two time steps, or a total of eight points. By the classic $\sqrt{N}$ ratio, this should reduce the noise floor by a factor of 2.8. This is roughly what is observed in Fig. 3.

The interpolated spectrum in each subplot of Fig. 3 precisely follows the original spectrum until about 100 kHz, then falls off to lower values. This is the point at which the lowered noise floor begins to have an appreciable effect. The decay of the spectrum rolls off to a steeper slope than could be measured using the noisier data.

The increased roll-off seen in the interpolated spectra plausibly may be attributed to a low-pass filtering effect of the interpolation process rather than a more accurate portrayal of the highest-frequency content as opposed. However, the treatment of Crochiere and Rabiner [19] indicates that this should not be anticipated to be the case. The steeper slope than the theoretical -5/3 value may be accurate if the turbulent fluctuations have not yet achieved isotropy; this is discussed at greater length subsequently. Nonetheless, the spectra from interpolated time series shown in Fig. 3 offer intriguing characteristics of increased effective frequency response due to a lower noise floor.

MHz-Rate Postage-Stamp PIV

Camera Performance

The most direct means of increasing the frequency limits of postage-stamp PIV is simply to run the laser and camera faster. Although the pulse-burst laser has been capable of MHz-rate measurements since its inception [20], the cameras used for the original 400-kHz postage-stamp PIV experiments had a hard limit of 480 kHz, and that for an unattractively small field of view. Improving technologies in high-speed cameras recently have produced the IX 726, which can reach MHz rates using approximately the same pixel count as in the previous experiments.

The advantage of a MHz-rate postage-stamp PIV system is not immediately obvious in that it cannot be expected to reduce the noise floor. In fact, it is understood that the noise actually is increased for such faster data transfers. But the increased framing rate will oversample the data for the frequencies of interest in the flow and therefore a conventional image-pair correlation to produce velocity vectors is no longer required to maintain frequency response. Instead, multiple-frame image interrogation may be used, of which a number of algorithms have been developed [21-27]. The increased accuracy of multiple-frame methods should lower the noise floor and therefore reveal higher-frequency content even well short of the Nyquist frequency of 500 kHz.

However, as indicated in the Experimental Configuration section, the IX 726 camera leaks charge through the shift register as a consequence of its MHz-rate capability. This tends to smear out the subject matter being viewed; for PIV images, this will create ghost particles. For the desired aspect ratio near unity, a field of view of 112 × 108 pixels is possible at 1 MHz. Figure 4 shows the effect of the charge leakage when viewing a resolution target; the unadulterated image is shown in Fig. 4a extracted from a full field of view at slower acquisition whereas Fig. 4b shows the distorted image due to the small image. Clearly, this is not a viable configuration for successful imaging.

The degree of shift leakage is dominantly a function of the horizontal dimension of the image. However, to maintain the required 1 MHz framing rate, the vertical dimension must be reduced to compensate. A 336 × 42 pixel field of view of the resolution target is shown in Fig. 4c and exhibits much less shift leakage than the 112 × 108 pixel

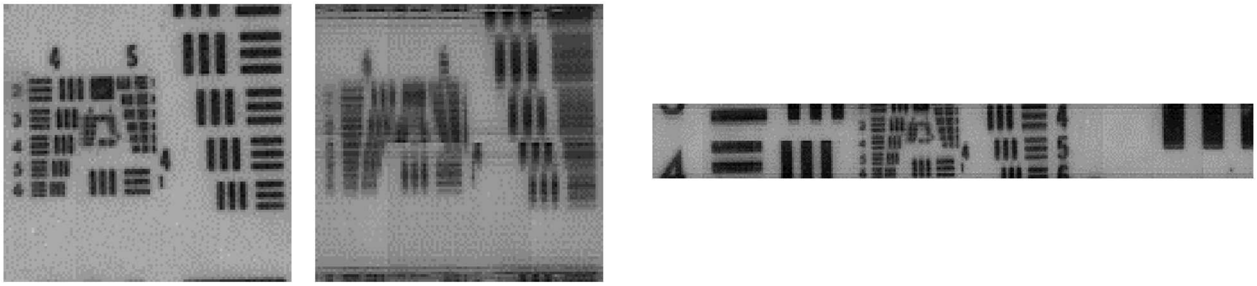

(a) (b) (c)

Fig. 4: Image distortion of a resolution target due to charge leakage through the shift register of the IX 726. (a) uncorrupted image (extracted from larger image) for a 112 × 108 pixel field of view; (b) shift leakage for a 112 × 108 pixel field of view; (c) shift leakage for a 336 × 42 pixel field of view.

field of view, though it is still present. For a 504 × 30 pixel field of view, the shift leakage is nearly negligible but the vertical dimension is becoming untenably small; this image is not shown.

Treating the shift leakage requires use of a high-aspect-ratio field of view rather than an approximately square field of view as in the 400-kHz postage-stamp PIV measurements. However, this has two consequences that are detrimental to PIV measurements. First, even aligned with the dominant convective direction, this presents the possibility of numerous particles leaving the field of view and increasing the measurement noise due to their loss. Worse, a bias error may occur if the most energetic motions, or the most vertically aligned motions, are selectively lost. Second, even with these high-aspect-ratio images, some amount of charge will leak between rows. This creates ghost particles in the images, which also can increase measurement noise and may create biases in the correlation peaks if the ghosts occur selectively in one direction. In fact, these ghost particles do occur aligned to the vertical direction because the leakage occurs across entire horizontal rows, mirrored above or below. The impact of both of these image features on PIV data quality must be tested.

Simulating Shift Charge Leakage

If the charge leakage through the camera shift register can be simulated in synthetic PIV images, the impact of this flaw on velocimetry measurements may be identified. But first, the characteristics of the shift leakage must be identified. To accomplish this, sequences of images of particles suspended in ambient room air were acquired for both 112 × 108 pixel and 336 × 42 pixel fields of view. Autocorrelations were found of the images and then averaged over each sequence, with the results given in Fig. 5 both as two-dimensional fields and as profiles sliced through the center of the correlation peaks.

Figure 5 shows that the ghosting occurs very repeatably spaced every third row. This is true for both fields of view (and others tested, though not shown). No ghosting displacement is observed along the x axis. The correlation magnitudes of the ghost peaks are considerably weaker for the 336 × 42 pixel case than for the 112 × 108 pixel case. In addition, tests have shown ghosting always occurs towards the horizontal centerline of the image, not in a uniform direction across the entire image. This can be observed in close inspection of Fig. 4c. But no ghosting occurs within a six-pixel core of the image where no shifting of charge is required prior to readout.

Magnitudes of the ghost images cannot be effectively determined by autocorrelations. Instead, images were acquired on the benchtop from grids of narrow lines or small dots, from which the ghost patterns were well separated and their intensities easily measured. By altering the lighting, the ghost intensity could be tracked as a function of image intensity and a relationship defined between the signal and ghost intensities. This relationship is shown in Fig. 6 for the 336 × 42 pixel field of view. Fourteen different cases are included in which the imaged lines or dots were located at different rows of the camera image, but no pattern could be found as a function of position on the camera array. Still, the data points scatter reasonably closely around a linear fit and this was used to define the intensity of ghost images.

As noted earlier, two effects needed to be captured by simulations of shift leakage. First, the effect of particle dropout through the narrow vertical extent of the images must be examined. And secondly, the presence of ghost particles upon the velocity data must be tested. Rather than generating synthetic PIV images, the actual PIV images from the 400-kHz data set were modified to simulate the effects of shift leakage. This allowed tests upon real PIV data and reduced the risk that the simulations may miss some relevant feature. The 128 × 112 pixel images native to the 400-kHz data simply were cropped top and bottom to reduce them to a narrow vertical extent, then reprocessed

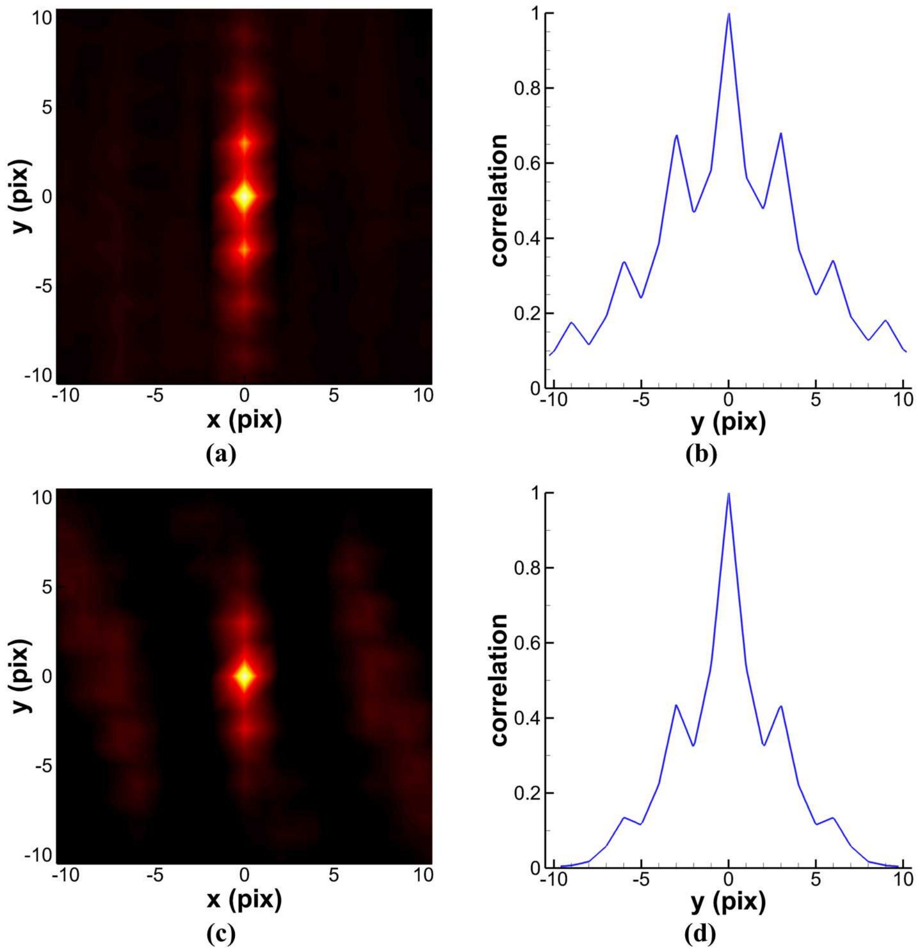

(a) (b) (c) (d)

Fig. 5: Autocorrelations of particle fields showing patterns of image ghosting; both two-dimensional fields and one-dimensional slices through the *x*=0 line are provided; (a, b) 112 × 108 pixel field of view; (c, d) 336 × 42 pixel field of view.

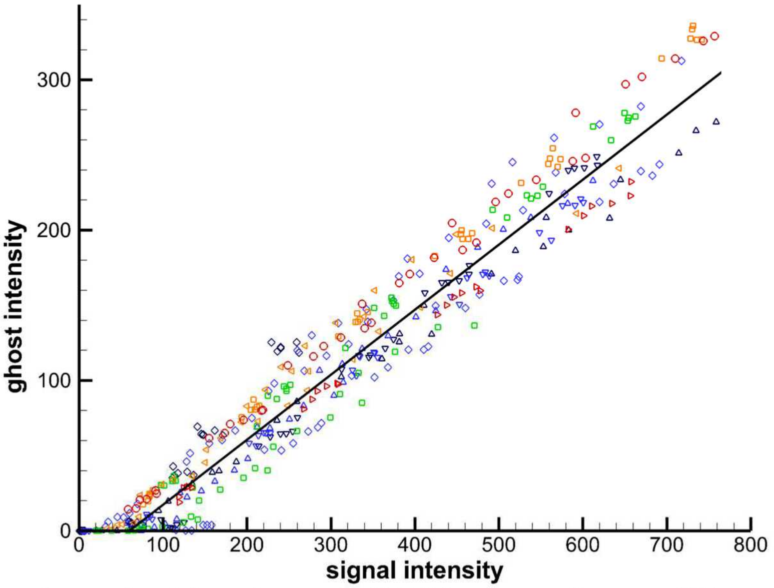

Fig. 6: Ghost intensity vs signal intensity on the IX 726 camera. Fourteen different camera rows are represented by the various data points but no trend between them was identified.

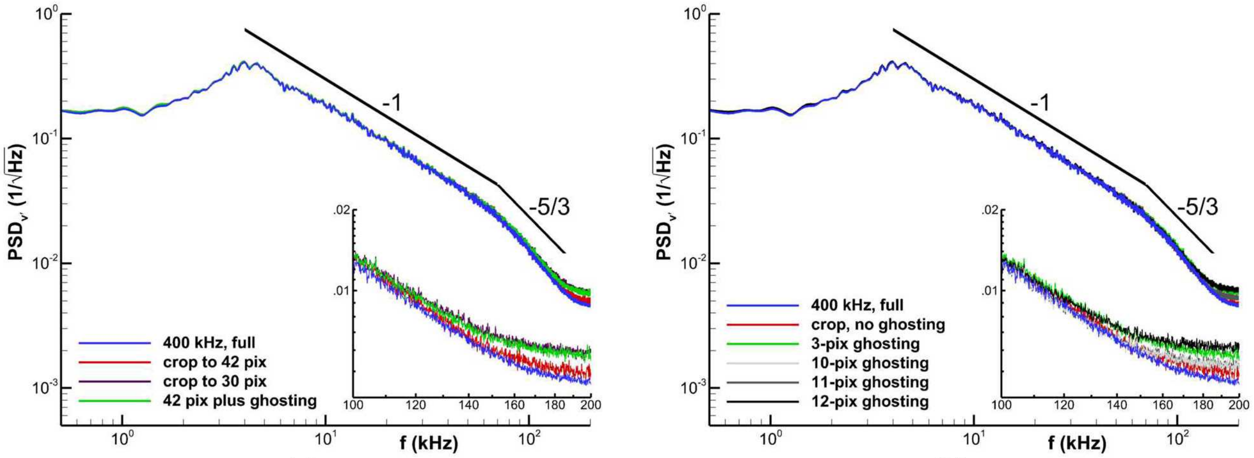

(a) **(b)**

Fig. 7: Power spectra from vertically cropped images of the 400-kHz postage-stamp PIV to simulate the IX 726 camera aspect ratios, as well as simulated ghosting due to shift register leakage.

through the PIV interrogation algorithm and compared to the original spectrum. The two image sizes tested in the present work at 990 kHz were 336 × 42 pixels and 504 × 30 pixels, so these two vertical extents were simulated from the 400-kHz data as well.

Figure 7a shows the results. The impact of a narrower image is seen only in an elevated noise floor at the highest frequencies, which is emphasized in the magnified scale of the inset plot. The noise floor rises just a little when cropped to a 42-pixel extent and rises somewhat further when cropped to 30 pixels. This is indicative of a greater number of particles departing the images in the narrower field of view. It also may reflect greater uncertainty when warping the narrow image between interrogation iterations where less information is available along a given axis. Regardless, a major impact to the spectrum is not observed and suggests that a significant problem is not posed by the size of the long, narrow field of view necessitated by the IX 726.

Also shown in Fig. 7a is a spectrum that crops the images to a 42-pixel extent and adds simulated ghosting. Ghosting was implemented by copying every particle outside the six-pixel centerline of the image, multiplying it by the image intensity relationship found in Fig. 6, then adding the resulting intensity to a pixel shifted three rows towards the centerline. This was performed on every image of every burst in the data set, then interrogated again for velocity vectors. No special analysis or additional vector validation was used to account for the ghost correlation peak. As Fig. 7a shows, the noise floor is elevated from the spectrum that is only cropped to 42 pixels but otherwise no distortion to the spectrum is created that would be indicative of a bias. From this, it is concluded that the shift register leakage adds noise but the camera is still serviceable for PIV.

At least, this conclusion is valid for the present flow, which is dominated by convection. The mean displacement of the flow is 12 pixels in the streamwise direction, with the smallest instantaneous displacement still more than half that value. Therefore, the signal correlation peak can be expected to always remain distant from the ghost correlation peak lying three pixels above or below the zero-displacement point. Might the ghost correlation interfere with the velocity measurement if the flow motion at some point in time is nearly three pixels vertically?

To answer this question, a flow would need to be tested with the IX 726 in an experimental configuration that induced particle displacements of three pixels vertically. Alternatively, to avoid crafting an experiment merely to answer this question, the simulated camera behavior was modified to suit the flow behavior for the present jet in crossflow. The ghost displacement was assumed to be 12 pixels in the horizontal direction rather than three pixels in the vertical direction, but otherwise exhibiting the same behavior as already observed. Thus an interference from the ghosting may be tested.

These results are given in Fig. 7b. Five different displacements were tested: 10, 11, 12, 13, and 14 pixels; this allowed a study of the sensitivity of the spectrum to the proximity of a ghost correlation peak. The latter two cases are omitted from the plot because they were found to be indistinguishable from the first two cases. When the ghost particles are near the mean flow displacement but not directly overlapping it (10- and 11-pixel ghosting) the noise floor is raised modestly but to a level less than that from a three-pixel ghost displacement. The noise probably falls below that of three-pixel ghosting because fewer ghost particles are present in an interrogation window when the ghost

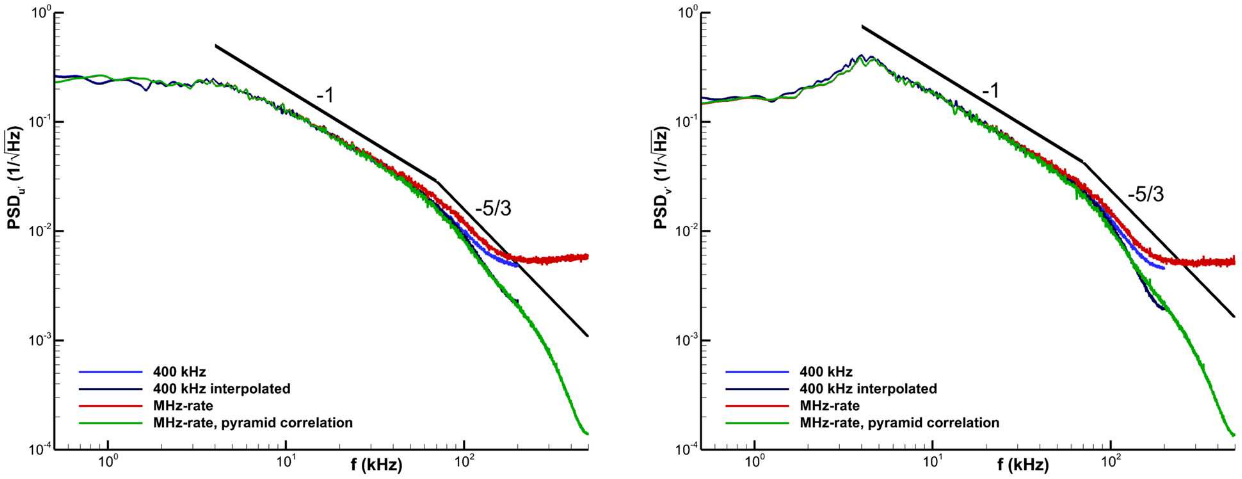

(a) **(b)**

Fig. 8: Power spectra from the MHz-rate postage-stamp PIV compared to the 400-kHz postage stamp PIV. The interpolated spectra of Fig. 3 are included for reference, as is analysis using the pyramid correlation [22] for the MHz-rate data. (a) streamwise component; (b) vertical component.

displacement is large. When the ghost particle displacement exactly matches the integer mean flow displacement (12-pixel ghosting), the noise floor rises further and exceeds that found from any other simulation. Nonetheless, this elevated noise is still relatively modest and importantly, no distortions to the spectrum are found that might be indicative of the presence of the ghost particles biasing the correlation. In short, the ghost particles do not “pull” the correlation to a fixed value that alters the spectrum. This indicates that even for flows in which the measured motion intersects with the ghosting due to shift leakage, the impact on the spectrum is mild and the IX 726 camera remains useful for PIV.

MHz-Rate PIV Results

Once the IX 726 camera was confirmed to be suitable for PIV despite its aspect ratio and shift register leakage, measurements were acquired of the jet-in-crossflow interaction. At 990 kHz and the 10.2-ms burst duration from the laser, about 10,100 frames were acquired per burst. Four bursts could be acquired per wind tunnel run and a little more than 30 tunnel runs were conducted for each of the 336 × 42 pixel and 504 × 30 pixel fields of view.

The MHz-rate postage-stamp PIV spectra are shown in Fig. 8 using the 336 × 42 field of view and are compared to the earlier 400-kHz spectra. At first glance, it does not appear that the MHz-rate data represent an improvement over the 400-kHz data. The noise floor actually is slightly higher from the MHz-rate data as a consequence of the narrow vertical extent and the particle ghosting as demonstrated in the previous sub-section (as well as the increased camera noise when transferring charge so rapidly). Though excluded from Fig. 8 for clarity, spectra acquired from the 504 × 30 field of view overlay the 336 × 42 spectra that are shown save that the noise floor is slightly higher, as predicted by Fig. 7.

Despite the modestly elevated noise floor, the MHz-rate data offer an important advantage: the increased framing rate provides oversampled data with respect to the frequencies of interest. This allows application of multi-frame interrogation algorithms [21-27]. Several different algorithms have been explored, but the pyramid correlation offers the most flexibility and accuracy [22]; results from it are added to Fig. 8. This algorithm functions by ensemble-averaging the correlation over multiple frames to improve its precision. The number of frames and their temporal separation are chosen at each time step through the image sequence to optimize the dynamic range and signal-to-noise ratio. Here, the pyramid correlation was conducted using N=5 frames and a maximum of two levels of correlations. Other parameters also have been explored but are omitted because their spectra exhibited characteristics of low-pass filtering; the results shown in Fig. 8 have proven most valuable.

Figure 8 shows that the noise floor is lowered by more than an order of magnitude when using the pyramid multi-frame correlation algorithm. With the greatly reduced interference from the noise floor, a region of roughly constant slope emerges for the *v* component in Fig. 8b beginning at approximately 80 kHz and extending perhaps to about 250-300 kHz where the slope diminishes yet again. This latter effect appears to be the point at which the spatial resolution limit due to the size of the interrogation window begins to noticeably filter the data. For the previous 400-kHz PIV, this was estimated to be 220 kHz [6]. The present camera configuration uses a magnification about 10% greater as

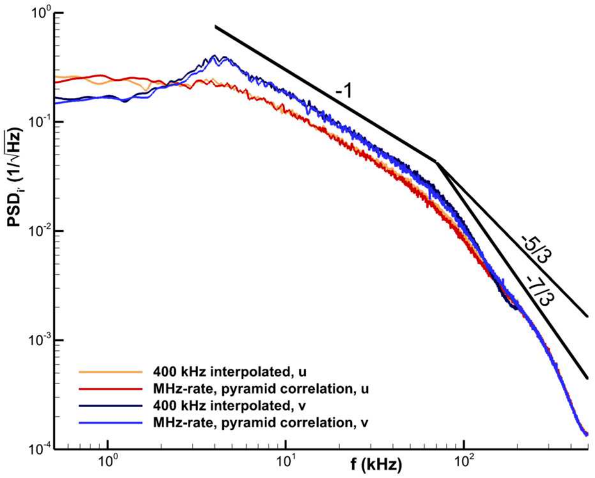

Fig. 9: Power spectra from Fig. 8 simultaneously plotting both *u* and *v* components along with possible scaling laws.

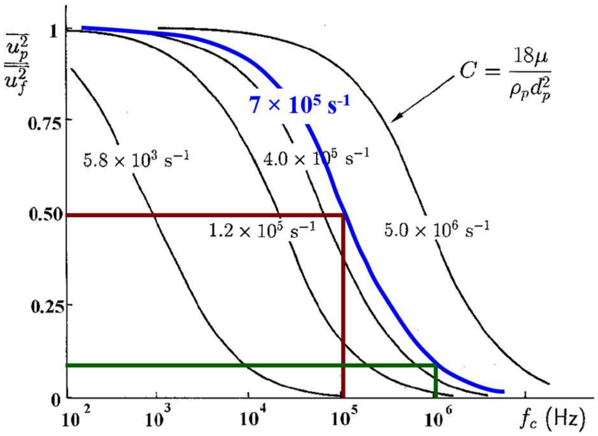

Fig. 10: Melling's Fig. 3 [47] of particle response time and velocity fluctuation sensitivity, annotated for conditions in the present experiment.

compared to the previous 400-kHz measurement, which reduces the spatial extent of an interrogation window and thereby raises its expected frequency response to 240 kHz. Similar effects are observed in the *u* component of Fig. 8a. Most encouragingly, the pyramid correlation analysis of the MHz-rate data aligns quite well with the interpolated 400-kHz spectra up to its limit at 200 kHz. The self-consistency suggests that both analysis methods are functioning well and returning valid spectra well beyond the previous effective frequency limit of about 120-130 kHz.

The slope beyond 70 kHz in both plots of Fig. 8 is steeper than that predicted by the -5/3 theory, but as noted earlier, this may be because the flow has not yet reached isotropy. Figure 9 provides both the *u* and the *v* components on the same plot to allow a direct comparison of the energy of the velocity fluctuations. In the high frequency range where onset of the inertial subrange may be expected, from about 70 kHz to perhaps 150 kHz, it can be seen that the spectrum for *v* has a larger magnitude than for *u*; therefore, the flow is not yet isotropic and a key assumption of the theoretical -5/3 slope has been violated. Therefore, the -5/3 slope of theory may not be descriptive of the present flow.

In fact, quite a number of studies both experimental and computational have established that even within the high-frequency range associated with the inertial subrange, anisotropic behavior may be found as well as intermittent behavior due to small-scale coherent structures passing through the flow [28-35]. As a consequence, the power-law slope has been found in some cases to deviate from the theoretical -5/3 value [33, 36-46]. In the present case, the *v* component proves a close match to -7/3 power-law behavior; the *u* component does not match this power quite so well though it is closer to -7/3 than it is to -5/3. Although several studies have indicated that the nonideal characteristics of anisotropy and intermittency should generate a steeper slope than -5/3, none suggest a slope as steep as found here nor do they provide reason to believe -7/3 is the correct value [36-39, 41-45].

The -7/3 slope of Fig. 9 may be no more than fortuitous – or it may indeed be accurate. Further validation of the multi-frame correlation techniques is warranted. The pyramid correlation has been shown to be more accurate than conventional two-frame correlation or a fixed-interval multi-frame correlation on a point-by-point basis [22], but its accuracy has not been evaluated in the spectral domain. Yet, its agreement with the interpolated 400-kHz data is striking. This matter lies beyond the scope of the present paper but an investigation currently is in progress. At this juncture, the MHz-rate PIV indicates that the inertial subrange power-law likely is steeper than -5/3, consistent with a number of low-speed studies, but the precise scaling law is not yet definitive.

Particle Response

The elevated frequency response of the MHz-rate PIV is only helpful if the particle response time can match it. *In situ* measurements of the particle response time have established a frequency response of 500-700 kHz, but application of Melling's analysis [47] or Mei's analysis [48] suggest the limitation may be 200 kHz or less when the energy contributions of fluctuations are considered. This is demonstrated in Fig. 10, which reproduces Melling's Fig. 3 and is annotated for conditions in the present experiment. Based on the measured particle size and flow characteristics, a curve representing the actual particles in the present flow is superposed. Mei suggests an appropriate, if semi-arbitrary, choice of frequency cutoff is that at which the energy response of the velocity fluctuations falls to 50%. This is marked by the brown line in Fig. 10 and corresponds to a frequency limit of 100 kHz; beyond this point, the measurements will lose sensitivity to the velocity fluctuations. This suggests the present MHz-rate measurements do not possess adequate particle response to achieve the measurements of behavior in the inertial subrange as exhibited by Fig. 9.

However, the intensity of velocity fluctuations at these high frequencies and small scales is much less than the maximum velocity fluctuations of the flow as a whole. This means such fluctuations contain considerably lower energy and do not require the same particle response to measure them. Examining any of the spectra presented herein, it can be seen that the energy at 100 kHz and above is at least an order of magnitude reduced from the peak energy of the flow. Re-examining Fig. 10, if only 10% of the peak energy must be measured, a higher frequency response is achieved. This is shown by the green line, suggesting that a particle frequency response of 1 MHz is possible should they need only measure velocity fluctuations of 10% of the peak. Therefore, the present measurements can achieve the superior particle response required for high-frequency content.

Conclusions

Two techniques have been developed to extend the effective frequency limits of postage-stamp PIV, in which a pulse-burst laser and very small fields of view are combined to achieve high repetition rates. One of these uses an interpolation scheme to provide a simple means of reducing the impact of measurement noise, which raises the effective frequency response of previous 400-kHz measurements from about 120 kHz to 200 kHz. The other technique increases the PIV acquisition rate to very nearly MHz rates (990 kHz), which never previously has been accomplished in a manner that can yield spectral content.

The MHz-rate measurement is achieved using a faster camera, but to achieve these framing rates it leaks charge through the shift register. To minimize this effect, it must be operated with a high aspect ratio. Existing PIV images were modified to simulate the camera performance. Their analysis established that the narrow vertical extent of the images and the ghost particles due to residual charge leakage both add a tolerable degree of noise to the measurements, but neither introduces any bias errors into the spectra. The increased framing rate provided oversampled data and enabled use of multi-frame correlation algorithms for increased measurement precision and a lower noise floor. The pyramid correlation increased the effective frequency response to at least 240 kHz, at which point the finite extent of the interrogation window is estimated to begin spatially filtering the data. Good agreement between the interpolation technique and the MHz-rate PIV measurements was established. Particle response time also was shown to be sufficient to measure velocity fluctuations at these very high frequencies.

The measured velocity spectra reveal the power-law scaling of the turbulence as the flow reaches the inertial subrange. Rather than displaying the theoretical -5/3 power-law scaling with frequency, the turbulent energy well matches a steeper power law and is suggestive of a value of -7/3. This is attributed to an absence of isotropy even in this high frequency range, which is a requirement of the -5/3 theory but is known not to be universally present in turbulent flows. The present very-high-frequency measurements establish the power of "postage-stamp PIV" to reveal turbulence scaling laws for compressible flows.

Acknowledgements

The authors would like to thank Todd Rumbaugh and Drew L'Esperance of Hadland Imaging for their assistance with the IX 726 camera. The authors also would like to thank John Henfling, recently retired from Sandia, for his contributions to earlier phases of this effort that made the present data possible.

References

[1] Ashok, A., Bailey, S. C. C., Hultmark, M., and Smits, A. J., "Hot-Wire Spatial Resolution Effects in Measurements of Grid-Generated Turbulence," *Experiments in Fluids*, Vol. 53, No. 6, 2012, pp. 1713-1722.

[2] Hutchins, N., Monty, J. P., Hultmark, M., and Smits, A. J., "A Direct Measure of the Frequency Response of Hot-Wire Anemometers: Temporal Resolution Issues in Wall-Bounded Turbulence," *Experiments in Fluids*, Vol. 56, No. 1, 2015, pp. 18.

[3] Benedict, L. H., Nobach, H., and Tropea, C., "Estimation of Turbulent Velocity Spectra from Laser Doppler Data," *Measurement Science and Technology*, Vol. 11, No. 8, 2000, pp. 1089-1104.

[4] Broersen, P. M. T., "Practical Aspects of the Spectral Analysis of Irregularly Sampled Data with Time-Series Models," *IEEE Transactions on Instrumentation and Measurement*, Vol. 58, No. 5, 2009, pp. 1380-1388.

[5] Beresh, S. J., Kearney, S. P., Wagner, J. L., Guildenbecher, D. R., Henfling, J. F., Spillers, R. W., Pruett, B. O. M., Jiang, N., Slipchenko, M., Mance, J., and Roy, S., "Pulse-Burst PIV in a High-Speed Wind Tunnel," *Measurement Science and Technology*, Vol. 26, No. 9, 2015, pp. 095305.

[6] Beresh, S. J., Henfling, J. F., and Spillers, R. W., "Postage-Stamp PIV: Small Velocity Fields at 400 kHz for Turbulence Spectra Measurements," *Measurement Science and Technology*, Vol. 29, No. 3, 2018, pp. 034011.

[7] Beresh, S. J., “Denoising 400-kHz ‘Postage-Stamp PIV’ using Uncertainty Quantification,” AIAA Paper 2018-2034, January 2018.

[8] Vetel, J., Garon, A., and Pelletier, D., “Denoising Methods for Time-Resolved PIV Measurements,” *Experiments in Fluids*, Vol. 51, No. 4, 2011, pp. 893-916.

[9] Gamba, M., and Clemens, N. T., “Requirements, Capabilities and Accuracy of Time-Resolved PIV in Turbulent Reacting Flows,” AIAA Paper 2011-0362, January 2011.

[10] Oxlade, A. R., Valente, P. C., Ganapathisubramani, B., and Morrison, J. F., “Denoising of Time-Resolved PIV for Accurate Measurement of Turbulence Spectra and Reduced Error in Derivatives,” *Experiments in Fluids*, Vol. 53, No. 5, 2012, pp. 1561-1575.

[11] Wieneke, B., “PIV Anisotropic Denoising using Uncertainty Quantification,” *Experiments in Fluids*, Vol. 58, No. 8, 2017, p. 94.

[12] Scarano, F., and Moore, P., “An Advection-Based Model to Increase the Temporal Resolution of PIV Time Series,” *Experiments in Fluids,* Vol. 52, No. 4, 2012, pp. 919-933.

[13] Wernet, M. P., and Opalski, A. B., “Development and Application of a MHz Frame Rate Digital Particle Image Velocimetry System,” AIAA Paper 2004-2184, January 2004.

[14] Brock, B., Haynes, R. H., Thurow, B. S., Lyons, G., and Murray, N. E., “An Examination of MHz Rate PIV in a Heated Supersonic Jet,” AIAA Paper 2014-1102, January 2014.

[15] Michaelis, D., Neal, D. R., and Wieneke, B., “Peak-Locking Reduction for Particle Image Velocimetry,” *Measurement Science and Technology*, Vol. 27, No. 10, 2016, pp. 104005.

[16] Beresh, S. J., Henfling, J. F., Erven, R. J., and Spillers, R. W., “Penetration of a Transverse Supersonic Jet into a Subsonic Compressible Crossflow,” *AIAA Journal*, Vol. 43, No. 2, 2005, pp. 379-389.

[17] Beresh, S. J., Wagner, J. L., Henfling, J. F., Spillers, R. W., and Pruett, B. O. M., “Turbulent Eddies in a Compressible Jet in Crossflow Measured using Pulse-Burst Particle Image Velocimetry,” *Physics of Fluids*, Vol. 28, No. 2, 2016, pp. 025102.

[18] Pope, S. B., *Turbulent Flows*, Cambridge University Press, 2000, pp. 228-242.

[19] Crochiere, R. E., and Rabiner, L. R., *Multirate Digital Signal Processing*, Prentice-Hall Inc., 1983.

[20] Thurow, B., Jiang, N., and Lempert, W., “Review of Ultra-High Repetition Rate Laser Diagnostics for Fluid Dynamic Measurements,” *Measurement Science and Technology*, Vol. 24, No. 1, 2013, pp. 012002.

[21] Hain, R., and Kähler, C. J., “Fundamentals of Multiframe Particle Image Velocimetry (PIV)”, *Experiments in Fluids*, Vol. 42, No. 4, 2007, pp. 575-587.

[22] Sciacchitano, A., Scarano, F., and Wieneke, B., “Multi-Frame Pyramid Correlation for Time-Resolved PIV,” *Experiments in Fluids*, Vol. 53, No. 4, 2012, pp. 1087-1105.

[23] Lynch, K., and Scarano, F., “A High-Order Time-Accurate Interrogation Method for Time-Resolved PIV,” *Measurement Science and Technology*, Vol. 24, No. 3, 2013, pp. 035305.

[24] Haynes, R. H., Brock, B. A., and Thurow, B. S., “Application of MHz Frame Rate, High Dynamic Range PIV to a High-Temperature, Shock-Containing Jet,” AIAA Paper 2013-0774, January 2013.

[25] Meinhart, C. D., Wereley, S. T., and Santiago, J. G., “A PIV Algorithm for Estimating Time-Averaged Velocity Fields,” *Journal of Fluids Engineering*, Vol. 122, No. 2, 2000, pp. 285-289.

[26] Westerweel, J., Elsinga, G. E., and Adrian, R. J., “Particle Image Velocimetry for Complex and Turbulent Flows,” *Annual Review of Fluid Mechanics*, Vol. 45, 2013, pp. 409-436.

[27] Scarano, F., Bryon, K., and Violato, D., “Time-Resolved Analysis of Circular and Chevron Jets Transition by Tomo-PIV”, *15th International Symposium on Applications of Laser Techniques to Fluid Mechanics*, Lisbon, Portugal, 2010.

[28] Mestayer, P., “Local Isotropy and Anisotropy in a High-Reynolds-Number Turbulent Boundary Layer,” *Journal of Fluid Mechanics*, Vol. 125, 1982, pp. 475-503.

[29] Saddoughi, S. G., and Veeravalli, S. V., “Local Isotropy in Turbulent Boundary Layers at High Reynolds Number,” *Journal of Fluid Mechanics*, Vol. 268, 1994, pp. 333-372.

[30] Kurien, S., and Sreenivasan, K. R., “Anisotropic Scaling Contributions to High-Order Structure Functions in High-Reynolds-Number Turbulence,” *Physical Review E*, Vol. 62, No. 2, 2000, pp. 2206-2212.

[31] Shen, X., and Warhaft, Z., “The Anisotropy of the Small Scale Structure in High Reynolds Number (R_λ= 1000) Turbulent Shear Flow,” *Physics of Fluids*, Vol. 12, No. 11, 2000, pp. 2976-2989.

[32] Biferale, L., and Toschi, F., “Anisotropic Homogeneous Turbulence: Hierarchy and Intermittency of Scaling Exponents in the Anisotropic Sectors,” *Physical Review Letters*, Vol. 86, No. 21, 2001, pp. 4831-4834.

[33] Tsuji, Y., “Large-Scale Anisotropy Effect on Small-Scale Statistics over Rough Wall Turbulent Boundary Layers,” *Physics of Fluids*, Vol. 15, No. 12, 2003, pp. 3816-3828.

[34] Pumir and Shraiman PRL 1995 Biferale, L., and Procaccia, I., “Anisotropy in Turbulent Flows and in Turbulent Transport,” *Physics Reports*, Vol. 414, 2005, pp. 43-164.

[35] Vassilicos, J. C., “Dissipation in Turbulent Flows,” *Annual Review of Fluid Mechanics*, Vol. 47, 2015, pp. 95-114.

[36] Anselmet, F., Gagne, Y., Hopfinger, E. J., and Antonia, R. A., “High-Order Velocity Structure Functions in Turbulent Shear Flows,” *Journal of Fluid Mechanics*, Vol. 140, 1984, pp. 63-89.

[37] She, Z.-S., and Leveque, E., “Universal Scaling Laws in Fully Developed Turbulence,” *Physical Review Letters*, Vol. 72, No. 3, 1994, pp. 336-339.

[38] Grossmann, S., Lohse, D., L’vov, V., and Procaccia, I., “Finite Size Corrections to High Reynolds Number Turbulence,” *Physical Review Letters*, Vol. 73, No. 3, 1994, pp. 432-435.

[39] Yoshizawa, A., "Nonequilibrium Effect of the Turbulent-Energy-Production Process on the Inertial-Range Energy Spectrum," *Physical Review E*, Vol. 49, No. 5, 1994, pp. 4065-4071.
[40] Mydlarski, L., and Warhaft, Z., "On the Onset of High-Reynolds-Number Grid-Generated Wind Tunnel Turbulence," *Journal of Fluid Mechanics,* Vol. 320, 1996, pp. 331-368.
[41] Wang, L.-P., Chen, S., Brasseur, J. G., and Wyngaard, J. C., "Examination of the Hypotheses in the Kolmogorov Refined Turbulence Theory through High-Resolution Simulations. Part 1. Velocity Field," *Journal of Fluid Mechanics*, Vol. 309, 1996, pp. 113-156.
[42] Ishihara, T., Yoshida, K., and Kaneda, Y., "Anisotropic Velocity Correlation Spectrum at Small Scales in a Homogeneous Turbulent Shear Flow," *Physical Review Letters*, Vol. 88, No. 15, 2002, pp. 154501.
[43] Kaneda, Y., Ishihara, T., Yokokawa, M., Itakura, K., and Uno, A., "Energy Dissipation Rate and Energy Spectrum in High Resolution Direct Numerical Simulations of Turbulence in a Periodic Box," *Physics of Fluids*, Vol. 15, No. 2, 2003, pp. L21-L24.
[44] Meyers, J., and Meneveau, C., "A Functional Form for the Energy Spectrum Parametrizing Bottleneck and Intermittency Effects," *Physics of Fluids*, Vol. 20, No. 6, 2008, pp. 065109.
[45] Horiuti, K., and Ozawa, T., "Multimode Stretched Spiral Vortex and Nonequilibrium Energy Spectrum in Homogeneous Shear Flow Turbulence," *Physics of Fluids*, Vol. 23, No. 3, 2011, pp. 035107.
[46] Ishihara, T., Morishita, K., Yokokawa, M., Uno, A., and Kaneda, Y., "Energy Spectrum in High-Resolution Direct Numerical Simulations of Turbulence," *Physical Review Fluids*, Vol. 1, No. 8, 2016, pp. 082403.
[47] Melling, A., "Tracer Particles and Seeding for Particle Image Velocimetry," *Measurement Science and Technology*, Vol. 8, No. 12, 1997, pp. 1406-1416.
[48] Mei, R , "Velocity Fidelity of Flow Tracer Particles," *Experiments in Fluids*, Vol. 22, No. 1, 1996, pp. 1-13.